pressure increases on the downstream side. A specimen for transmission electron microscopy (TEM) was prepared by sectioning a hybrid nanocomposite containing 10 wt.-% FS at –100 °C in a Reichert-Jung cryo-ultramicrotome. Electron-transparent sections measuring ca. 80 nm thick were imaged with a Zeiss EM902 electron spectroscopic microscope operated at an accelerating voltage of 80 kV and an energy loss of 0 eV.

Received: September 5, 2002
Final version: December 12, 2002

[1] W. C. Kratz, D. L. Rarig, J. M. Pietratonio, *AIChE Symp. Ser.* **1988**, *84*, 36.
[2] A. Kohl, R. Nielson, *Gas Purification*, Gulf Publishing Co., Houston, TX **1997**.
[3] R. M. de Vos, H. Verweij, *Science* **1998**, *279*, 1710.
[4] A. Tavolaro, E. Drioli, *Adv. Mater.* **1999**, *11*, 975.
[5] V. I. Bondar, B. D. Freeman, I. Pinnau, *J. Polym. Sci. B: Polym. Phys.* **2000**, *38*, 2051.
[6] J. H. Kim, S. Y. Ha, Y. M. Lee, *J. Membr. Sci.* **2001**, *190*, 179.
[7] *Chem. Eng. News* **2002**, *June 24*, pp. 61–62.
[8] S. Young, *Nature* **2001**, *414*, 487.
[9] J. M. Ogden, *Phys. Today* **2002**, *55*, 69.
[10] S. H. Lin, C. T. Shyu, *Environ. Technol.* **2000**, *21*, 1245.
[11] B. D. Freeman, I. Pinnau, *Trends Polym. Sci.* **1997**, *5*, 167.
[12] A. Morisato, I. Pinnau, *J. Membr. Sci.* **1996**, *121*, 243.
[13] T. Graham, *Philos. Mag.* **1866**, *32*, 401.
[14] V. P. Shantarovich, I. B. Kevdina, Y. P. Yampolskii, A. Y. Alentiev, *Macromolecules* **2000**, *33*, 7453.
[15] B. D. Bhide, S. A. Stern, *J. Membr. Sci.* **1993**, *81*, 209.
[16] I. W. Hamley, *The Physics of Block Copolymers*, Oxford University Press, New York **1998**.
[17] R. M. Barrer, in *Diffusion and Permeation in Heterogeneous Media* (Eds: J. Crank, G. S. Park), Academic Press, London and New York **1968**, p. 165.
[18] Y. Hirayama, Y. Kase, N. Tanihara, Y. Sumiyama, Y. Kusuki, K. Haraya, *J. Membr. Sci.* **1999**, 160, 87.
[19] L. M. Robeson, *J. Membr. Sci.* **1991**, *62*, 165.
[20] L. van de Beld, K. R. Westerterp, *AIChE J.* **1996**, *42*, 1139.
[21] T. J. Pinnavaia, *Science* **1983**, *220*, 365.
[22] C. Maxwell, *Treatise on Electricity and Magnetism*, Oxford University Press, London **1873**, *3*, Vol. 1.
[23] T. C. Merkel, B. D. Freeman, R. J. Spontak, Z. He, I. Pinnau, P. Meakin, A. J. Hill, *Science* **2002**, *296*, 519.
[24] H. J. Walls, J. Zhou, J. A. Yerian, P. S. Fedkiw, S. A. Khan, M. K. Stowe, G. L. Baker, *J. Power Sources* **2000**, *89*, 156.
[25] M. B. Shiflett, H. C. Foley, *Science* **1999**, *285*, 1902.

Shear and Young's Moduli of MoS_2 Nanotube Ropes**

By *András Kis*, *Dragan Mihailovic*, *Maja Remskar*, *Ales Mrzel*, *Adolf Jesih*, *Ireneusz Piwonski*, *Andrzej J. Kulik*, *Willy Benoît*, *László Forró**

In the past decade, the discovery of fullerenes and carbon nanotubes as new forms of carbon has prompted the opening of an interesting and dynamic new field in physics, chemistry, and materials science because of their remarkable properties and a wide range of potential applications. With the discovery of tungsten disulfide (WS_2) and molybdenum disulfide (MoS_2) fullerene-like nanoparticles and tubular structures,[1,2] followed by the discovery of boron nitride (BN) nanotubes,[3] it was realized that fullerenes and carbon nanotubes represent only a small subset of a wide class of layered materials that can form C_{60}-like particles, tubes, and other interesting morphologies.

MoS_2 can be synthesized in a large variety of forms—particles, nanotubes,[1,2] multiwalled nanotubes[4] and also—like their carbon cousins—in the form of ropes, ribbons, and thin microtubes several micrometers in diameter and millimeters in length.[5] This richness in form promises potential applications going beyond those of carbon nanotubes.

Recent theoretical calculations[6] predicted that MoS_2 nanotubes with diameters above 2 nm will all be semiconductors with a bandgap smaller than that of bulk MoS_2. The size of this gap is a monotonous and smooth function of the tube's diameter and chirality. Zigzag tubes would even have a small direct gap, suggesting that they could be used for optoelectronics i.e., luminescent devices, which is not possible for carbon nanotubes. At this time, there are no theoretical calculations available on MoS_2 nanotubes with subnanometer diameters, such as the ones used in this study. Nevertheless, recent experimental findings indicate that these tubes are most likely all metallic.[7,8]

Carbon nanotubes are always produced with a distribution of diameters and chiralities over which there is no real control. As a consequence, they have diverse electronic properties: semiconducting p- and n-tubes are produced along with metallic ones. Even a small change of diameter can drastically alter their electronic properties from metallic to semiconducting. In order to control the electronic properties of carbon nanotubes during production, complete control over their diameters is needed—a feat that has not been achieved yet. A narrow distribution of diameter will still yield a mixture of metallic and semiconducting tubes. MoS_2 nanotubes on the other hand do not require perfect control over their diameters, because they are predicted to be semiconductors with a monotonous dependence of the bandgap on the diameter. Thanks to this, perfect control over their diameter is not needed: a narrow distribution in their diameter would result in only a narrow distribution of the bandgap.

Nevertheless, a new type of single-walled MoS_2 synthesis[9] reproducibly yields bulk quantities of identical tubes, individually all 0.96 nm in diameter—corresponding to (3,3) chirality—but stuck together in ropes or bundles. These assemblies can be up to many tens of micrometers long and are composed of up to 10^6 individual tubes. The fact that they all have exactly the same diameter and therefore uniform electronic properties makes them very interesting for potential applications in nanoscale electronics.

Similarly to graphite, MoS_2 and WS_2 are characterized by weak (van der Waals) interatomic interactions between their layered structures, allowing easy, low strength shearing.[10] Therefore, it came as almost no surprise that MoS_2 and WS_2

[*] Prof. L. Forró, A. Kis, Dr. I. Piwonski, A. J. Kulik, Prof. W. Benoît
Institut de la physique de la matière complexe, EPFL
CH-1015 Lausanne (Switzerland)
E-mail: laszlo.forro@epfl.ch
Prof. D. Mihailovic, Dr. M. Remskar, Dr. A. Mrzel, Dr. A. Jesih
Jozef Stefan Institute
Jamova 39, SL-1000 Ljubljana (Slowenia)

[**] We thank G. Beney for polishing the Al_2O_3 membranes together with J.-P. Salvetat and G. A. D. Briggs for interesting discussions. The access to electron microscopes was kindly provided by the Centre Interdépartemental de Microscopie Electronique (CIME) at the EPFL.

 DOI: 10.1002/adma.200304549

ADVANCED MATERIALS

nanoparticles behave as exceptional solid-state lubricants,[11] with very low friction coefficient (between 0.008 and 0.01) and excellent wear resistance.[12] Apart from their use as lubricants in niche applications where liquid lubricants are impractical (such as space and ultrahigh vacuum), the low value of friction between neighboring layers of MoS_2 makes MoS_2 nanotubes interesting for future nanoscale mechanical systems, i.e., bearings. Besides, MoS_2 could prove to be a valuable system for studying fundamental physical properties of low-dimensional (in this case 1D) systems. One very convenient way of studying mechanical intertube interaction is by measuring the mechanical properties of MoS_2 nanotube bundles. The shear modulus of ropes would give an insight into the strength of connection between individual tubes comprising the rope.

The single-walled MoS_2 nanotubes used in our studies were produced by means of a catalyzed transport method. C_{60} (5 wt.-%) was added to MoS_2 powder in the transport tube as catalyst, and the reaction was run typically for 22 days at 1000 K in an evacuated silica ampoule at a pressure of 10^{-3} Pa with a temperature gradient of 6 K cm^{-1}. Iodine was used as a transport agent. Under these experimental conditions, approximately 15 % of the starting material formed single-walled tubes in the form of bundles with iodine intercalated between the individual tubes. High-resolution transmission electron microscopy (HRTEM) studies have revealed that the diameter of individual tubes is 0.96 nm.[9] Further heating at 800 °C of the MoS_2 material in the stream of H_2 results in the removal of the intercalated iodine[13] and ropes that can easily be dispersed in ethanol using ultrasound. The resulting ropes have a highly ordered structure as can be seen from the TEM image shown in Figure 1a. During the sonication process "nanorings" of MoS_2 like the one shown on Figure 1b can form when a MoS_2 rope wraps around a bubble in the agitated liquid.

The measurement method we used was developed in our group by Salvetat et al. for measurements on carbon nanotubes.[14] It consists of elastically deforming a beam (NT rope) firmly held on each end. The normal force is applied using an atomic force microscope (AFM) and changes in the tube's vertical deflection are measured.[14]

Ropes of MoS_2 composed of individual tubes, all 0.96 nm in diameter, were dispersed in absolute ethanol using ultrasound for a period of 15 min and were then deposited on a surface of a polished Al_2O_3 ultrafiltration membrane (Whatman anodisc) with mean pore size of 200 nm. By chance, nanotube ropes occasionally lie over pores (Fig. 1c) and are firmly held in place by surface adhesion. During extended AFM imaging no movement of the portions of the nanotube rope in contact with the filter is observed, allowing us to use the clamped beam model for describing their deformation. As an AFM, we used a Thermomicro M5 operating in air and equipped with capacitive displacement sensors and a closed-loop feedback for piezo scanner movement calibration and linearization, enabling accurate positioning. The AFM lever was Si_3N_4 (Thermomicro sharpened microlever) with a nominal force constant between 0.03 and 0.1 N m^{-1}. The force constant was calibrated by measuring the resonance frequency in air.[15] When a suitable rope, composed of several identical nanotubes is found, a series of AFM images is taken under varying load. The rope's diameter (d), suspended length (L), and vertical deflection in the middle (δ) are determined directly from AFM images such as the one shown in Figure 1c. Due to convolution of the rope with the AFM tip, the rope appears broadened; therefore, we use rope's height as an accurate measure of its diameter. As no change in rope height under different loads is observed, we can neglect deformation due to normal force. A typical deflection (δ) versus force (F) data set is given in Figure 1d. The reversibility of the curve and its linearity indicate that the deflection is elastic and linear for the experimental range of applied forces and measured deflections.

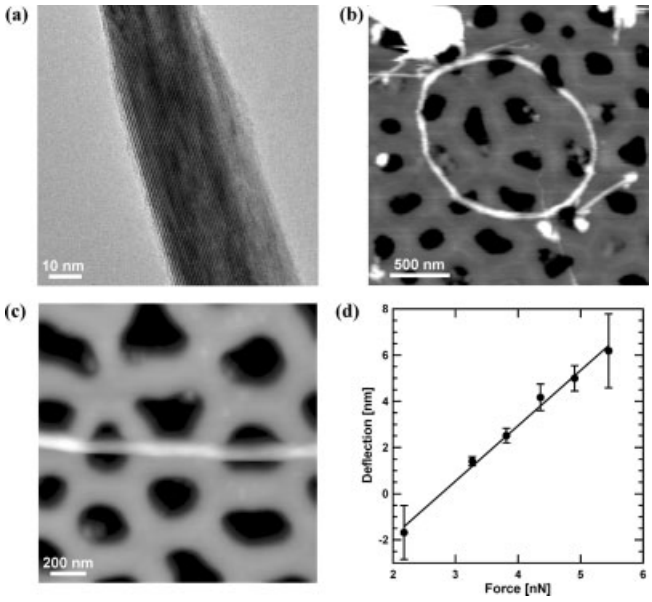

Fig. 1. a) TEM image of a single rope of MoS_2 nanotube after heat treatment in H_2. The image was obtained using a Philips CM-20 TEM operating at 200 kV. b) AFM image of a MoS_2 "nanoring" formed during sonication of the suspension containing MoS_2 nanotubes. The tube's diameter is 12 nm, and the ring's diameter is 1.5 μm. c) AFM image of an MoS_2 rope lying over two pores. The rope's diameter is 17 nm. d) A typical deflection vs. force curve obtained from a series of AFM images similar to those in (c), under varying normal load.

Small deformation of an elastic beam as a function of applied load can be calculated using the unit load method[16] and, in general, consists of bending (δ_B) and shearing (δ_S) deformation. The total deformation is the sum of these two and is given by Equation 1

$$\delta = \delta_B + \delta_S = FL^3/192EI + f_sFL/GA = FL^3/192E_{bending}I \qquad (1)$$

where F is the applied normal force, L the suspended length of the tube, E the Young's modulus, I the second moment of the area ($I = \pi D^4/64$), f_s the shape factor (equal to 10/9 for a cylindrical beam), G the shear modulus, A the area of the cross section, and D the external diameter of the nanotube rope (bundle). The result of a single bending experiment is

$E_{bending}$, the effective bending modulus of the rope, which would be equal to the Young's modulus if the effect of shearing was neglected. The contribution of shearing to the total deformation can be neglected in the case where E and G are of similar orders of magnitude. In other words, $E_{bending}$ would be close to E in the case where the rope's diameter would be much smaller than the suspended length.

The ropes (bundles) are composed of several tubes (all with the same diameter), and the rope's external diameter changes with the number of tubes comprising the rope. Young's modulus (E) describes the resistance of the entire rope to stretching, while the shear modulus (G) describes the sliding between individual tubes comprising the rope (Fig. 2, inset). We anticipate a numerical value of G that is much smaller than E, as expected from the low friction coefficient.[11] By measuring the elastic response of ropes with different diameters, corresponding to a different number of individual tubes that have bundled together in the rope, one can vary the relative weight of the two terms in Equation 1 corresponding to stretching and shearing. Ropes with a different number of tubes will have different contributions to the mechanical deformation coming from shearing and from stretching. Measurements have to be performed on several ropes with varying external diameters in order to extract the numerical values of the Young's and the shear modulus. The experimental error in determining the suspended length is estimated to be around 15 %, so $E_{bending}$ can be measured with 50 % precision.

For convenience, $E_{bending}$ from Equation 1 can be written as:

$$1/E_{bending} = 1/E_{Young} + (10/3G)(D^2/L^2) \quad (2)$$

The variation of $1/E_{bending}$ has been plotted as a function of D^2/L^2 for 13 ropes with different external diameters in Figure 2. From the slope of the fitted line the value of the shear modulus $G = 160 \pm 30$ MPa is obtained. The value of $E_{bending}$ for the thin, long ropes is expected to be close to E, so we also estimate that the lower limit of the Young's modulus E is 120 GPa—the value found for the rope with the lowest D/L ratio. For comparison, nanoindentation studies performed on sputtered MoS_2 films gave a Young's modulus around 160 GPa.[17] Unfortunately, there are no theoretical calculations available in the literature for MoS_2 nanotubes that could be used for comparison.

The low value of shear modulus is rather exceptional—as a comparison, the interlayer shear modulus of graphite is 4.5 GPa, and the shear modulus of carbon nanotubes is 1–10 GPa[18] (Table 1). In the case of MoS_2, the tubes' outer surface is composed of sulfur atoms. Their weak interaction could explain this rather low value of the intertube shear modulus.

Table 1. Comparison of the Young's and shear moduli for graphite, carbon, and MoS_2 ropes. For graphite, the in-plane Young's and the interplane shear moduli are given.

Material	Young's modulus E [GPa]	Shear modulus G [GPa]
Graphite	1060	4.5
Carbon SWNT ropes	1200	1–10
MoS_2 ropes	120	0.16

To conclude, we have used a nano-beam configuration in which ropes of MoS_2 were dispersed on the surface of a porous membrane. An AFM was engaged to elastically deform the ropes and the value of bending modulus was measured for an ensemble of tubes. From these measurements, the lower estimate for the Young's modulus of MoS_2 tubes was extrapolated as 120 GPa and the value of the inter-tube shear modulus was found to be 160 ± 30 MPa, indicating that MoS_2 ropes are highly anisotropic, and that the interaction between individual tubes comprising the rope is very weak.

Received: October 25, 2002
Final version: January 8, 2003

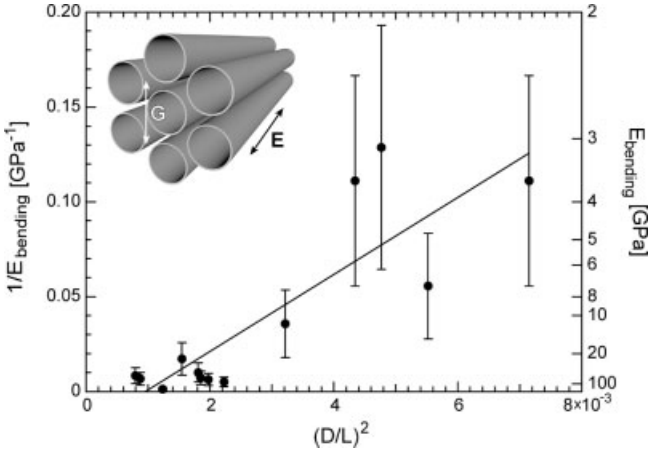

Fig. 2. The plot of inverse $E_{bending}$ measured for 13 different MoS_2 ropes, as a function of the ropes' geometry (total external diameter D divided by the length of the suspended rope). The value of $E_{bending}$ varies due to intertube shearing. The shear modulus G can be obtained from the slope of the linear fit. Inset: The nanotube rope, composed of several individual tubes in the continuous beam approximation. Young's modulus (E) describes the resistance of the entire rope to stretching, while the shear modulus G describes the sliding between individual tubes comprising the rope.

[1] R. Tenne, L. Margulis, M. Genut, G. Hodes, *Nature* **1992**, *360*, 444.
[2] L. Margulis, G. Salitra, R. Tenne, M. Talianker, *Nature* **1993**, *365*, 113.
[3] N. G. Chopra, R. J. Luyken, K. Cherrey, V. H. Crespi, M. L. Cohen, S. G. Louie, A. Zettl, *Science* **1995**, *269*, 966.
[4] M. Nath, A. Govindaraj, C. N. R. Rao, *Adv. Mater.* **2001**, *13*, 283.
[5] M. Remskar, Z. Skraba, F. Cléton, R. Sanjinés, F. Lévy, *Appl. Phys. Lett.* **1996**, *69*, 351.
[6] G. Seifert, H. Terrones, M. Terrones, G. Jungnickel, T. Frauenheim, *Phys. Rev. Lett.* **2000**, *85*, 146.
[7] C. Schönenberger, unpublished.
[8] P. Avouris, unpublished.
[9] M. Remskar, A. Mrzel, Z. Skraba, A. Jesih, M. Ceh, J. Demsar, P. Stadelmann, F. Levy, D. Mihailovic, *Science* **2001**, *292*, 479.
[10] R. G. Dickinson, L. Pauling, *J. Am. Chem. Soc.* **1923**, *45*, 1466.
[11] L. Rapoport, Y. Bilik, Y. Feldman, M. Homyonfer, S. R. Cohen, R. Tenne, *Nature* **1997**, *387*, 791.
[12] M. Chhowalla, G. A. J. Amaratunga, *Nature* **2000**, *407*, 164.
[13] D. Mihailovic, unpublished.
[14] J.-P. Salvetat, A. J. Kulik, J.-M. Bonard, G. A. D. Briggs, T. Stöckli, K. Méténier, S. Bonnamy, F. Béguin, N. A. Burnham, L. Forró, *Adv. Mater.* **1999**, *11*, 161.
[15] J. P. Cleveland, S. Manne, D. Bocek, P. K. Hansma, *Rev. Sci. Instrum.* **1993**, *64*, 403.

ADVANCED MATERIALS

[16] J. M. Gere, S. P. Timoshenko, *Mechanics of Materials*, PWS-Kent, Boston, MA **1990**.
[17] T. L. Mogne, C. Donnet, J. M. Martin, A. Tonck, N. Millard-Pinard, S. Fayeulle, N. Moncoffre, *J. Vac. Sci. Technol. A* **1994**, *12*, 1998.
[18] J.-P. Salvetat, G. A. D. Briggs, J.-M. Bonard, R. R. Bacsa, A. J. Kulik, T. Stöckli, N. Burnham, L. Forró, *Phys. Rev. Lett.* **1999**, *82*, 944.

Reversible Formation and Decomposition of LiF Clusters Using Transition Metal Fluorides as Precursors and Their Application in Rechargeable Li Batteries**

By *Hong Li*,* *Gunther Richter*, and *Joachim Maier*

Whether a solid material can take part in an electrochemical reaction is, besides thermodynamic constraints, determined by kinetic factors, such as the rate of charge transfer and transport within the bulk and across the interface. In view of low electronic and ionic conductivity, Li_2O has been regarded as an electrochemical inactive material at room temperature. However, recent studies of Tarascon's group show that if Li_2O is dispersed with transition metal elements (M = Fe, Co, Ni, Cu) on a nanoscale, Li can be electrochemically extracted from M/Li_2O nanocomposites.[1,2] This surprising and technologically highly relevant finding may be due to the reduced transport pathways, the interface chemistry and/or size effects on these properties.[3,4]

It is known that discharging a Li/MO_x cell can transform the metal oxide in situ into a M/Li_2O nanocomposite.[5–6] In this way, Li can be reversibly stored in lithium batteries by forming and decomposing Li_2O using transition metal oxides as precursors:[1,2,7,8]

$$MO_x + 2Li^+ + 2e^- \rightleftarrows M/Li_2O \quad (1)$$

In view of technological application, it is significant to note that the nanocomposite need not be pre-fabricated but forms during the insertion of lithium into the transition metal oxide.

Like Li_2O, LiF is also known as a poor electronic and ionic conductor at room temperature,[9] and particularly strong bonds are formed between lithium and fluorine (the electronegativity difference between lithium and fluorine is 3, compared to 2.5 for Li_2O). Hence it has never been reported to be electrochemically active in a Li cell. It is naturally very relevant to find out whether transition metal fluorides can show a similar electrochemical behavior and whether the very stable LiF can be reversibly decomposed if dispersed with transition metals on an atomic or nanometer scale.

[*] Dr. H. Li, Prof. J. Maier
Max-Planck-Institut für Festkörperforschung
Heisenbergstr.1, D-70569 Stuttgart (Germany)
E-mail: h.li@fkf.mpg.de
Dr. G. Richter
Max-Planck-Institut für Metallforschung
Heisenbergstr. 5, D-70569 Stuttgart (Germany)

[**] We thank H. Vogt, A. Fuchs, and G. Götz for help in micro-Raman, SEM, and XRD measurements; P. Balaya and J. Jamnik for helpful discussion.

The electrochemical reaction of metal fluorides with Li and its reverse reaction may be written as:

$$MF_n + nLi^+ + ne^- \rightleftarrows M/LiF \quad (2)$$

The emf values of above reactions are calculated for various metal fluorides (M = Ti, V, Mn, Fe, Co, Ni, Cu, Zn, Ag, Sn) according to Nernst equation (interfacial energy has been neglected) from thermodynamic data[10] and listed in Table 1. All the metal fluorides considered here naturally exhibit a lower reaction voltage than the decomposition voltage of 6.1 V for pure LiF, but higher values, by about 1 V, than the corresponding metal oxides. In view of thermodynamics, it is still possible to investigate the above reactions in common nonaqueous electrolyte systems with an electrochemical window of a width of 5 V. In addition, according to Table 1, most transition metal fluorides show theoretical gravimetric capacities which are comparable to the transition metal oxides, but much higher than for graphite (< 372 mA h g^{-1}), which has been used as anode material in commercial Li ion batteries.

Table 1. EMF of the electrochemical reactions between various metal fluorides and lithium and their corresponding Li storage capacity.

MF_n	ΔG_f [kJ]	$E°$ [V]	Capacity [mA h g^{-1}]	MF_n	ΔG_f [kJ mol^{-1}]	$E°$ [V]	Capacity [mA h g^{-1}]
AgF	–187	4.156	211	FeF_3	–972	2.742	712
CoF_3	–718	3.617	694	ZnF_2	–713	2.404	518
CuF_2	–491	3.553	528	MnF_2	–807	1.919	577
SnF_2	–601	2.984	342	VF_3	–1226	1.863	745
NiF_2	–604	2.964	554	TiF_3	–1361	1.396	767

Hence, we found it relevant to investigate the electrochemical reactions of MF_n (M = Ti, V, Mn, Fe, Co, Ni, Cu, Zn, Ag, Sn; $n = 2$ or 3) with lithium at room temperature. In this communication, we report mainly the results of TiF_3 and VF_3 in view of their advantageous electrochemical performances.

The voltage profiles of a Li/TiF_3 cell are shown in Figure 1. Three electrochemical reaction regions are observed during the discharging process (Li insertion, voltage decreases) and

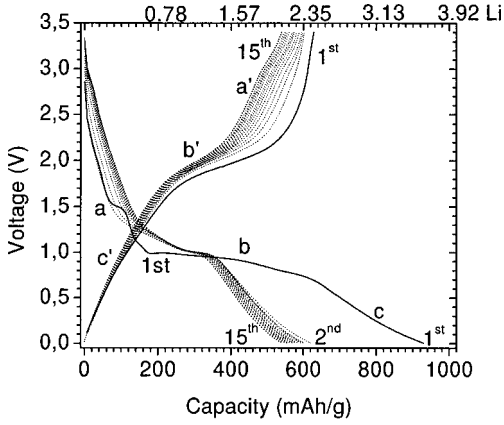

Fig. 1. Voltage profiles of a Li/TiF_3 cell cycled between 20 mV and 3.5 V. The letters designate different electrochemical reaction regions (explained in text).

  DOI: 10.1002/adma.200304574